



# On the westward shift of tropical Pacific climate variability since 2000

Xiaofan Li<sup>1</sup> · Zeng-Zhen Hu<sup>2</sup> · Emily Becker<sup>2</sup>

Received: 6 November 2018 / Accepted: 2 February 2019 / Published online: 21 February 2019

© This is a U.S. government work and its text is not subject to copyright protection in the United States; however, its text may be subject to foreign copyright protection 2019

## Abstract

A profound westward shift in atmosphere–ocean variability in the tropical Pacific is observed when 2000–2017 is compared to 1979–1999. This westward displacement is associated with changes in oceanic Kelvin wave activity along the equator, especially a remarkable reduction in the eastern Pacific (175°–145°W). This coincides with a weakening of low-level westerly winds in this region, and a westward shift of low-level easterly winds in the central and eastern tropical Pacific, as well as decreased variability of vertical entrainment, vertical diffusion in the ocean mixed-layer in the eastern Pacific. The observed enhancement of the zonal contrast of the mean state across the tropical Pacific seems to be associated with the westward shift of climate variability along the equator. This systematically westward shift of the atmosphere–ocean variability in the tropical Pacific alters the impact of the tropical Pacific on extra-tropical climate.

**Keywords** Westward shift of tropical Pacific variability · Oceanic Kelvin wave activity · Zonal gradient of SST

## 1 Introduction

The El Niño–Southern Oscillation (ENSO) is a major player for interseasonal to interannual time scale climate variability and predictability (National Research Council 2010; Chiodi and Harrison 2015; Wang et al. 2016). Therefore, understanding ENSO is crucial for successful forecasting of extratropical climate anomalies in many regions. While model development and observing systems have progressed in recent decades, the prediction skill of ENSO has not shown steady improvement, and in fact has declined (Wang et al. 2010; Barnston et al. 2012). This decline in prediction skill may be mainly due to changes in the characteristics of ENSO.

One of most significant changes is the decrease of ENSO variability since 1999/2000 (McPhaden 2012; Hu et al. 2013, 2017a), which also coincides with a suppression of subsurface ocean temperature variability and a weakening of atmosphere–ocean coupling in the tropical Pacific (Kumar

and Hu 2014; Hu et al. 2016). The decline of ENSO prediction skill may also be associated with a so-called breakdown of the relationship between the warm water volume (WWV) integrated along the equatorial Pacific and sea surface temperature (SST) anomalies (SSTAs) of ENSO (McPhaden 2012; Horii et al. 2012; Kumar and Hu 2014; Wen et al. 2014; Hu et al. 2017a), as well as the increased occurrence of so-called central Pacific (CP) ENSO (Yeh et al. 2009; Yu et al. 2011; Ren and Jin 2011; Capotondi et al. 2015). In the period prior to 1999/2000, WWV anomalies would occur 6–8 months before an ENSO event; since 2000, this lead time has been on the order of 2–3 months (McPhaden 2012). Both McPhaden (2012) and Horii et al. (2012) speculated that this breakdown may be associated with the contemporaneous shift towards more CP versus eastern Pacific (EP) El Niño events, and may also affect the relative importance of feedback mechanisms associated with ENSO variability.

Recently, Hu et al. (2017a, b) documented that the shortening of lead time is in fact due to frequency increases in both WWV variability and ENSO. The dominant frequencies were 1.5–3.5 years for both the Niño3.4 and WWV indices during 1979–1999. In contrast, both indices displayed a relatively flatter spectrum, similar to a white noise process, with a smaller peak of power spectrum at time scales shorter than 2.0 years during 2000–2016. Hu et al. (2017b) further argued that the frequency changes of ENSO and WWV are linked to a westward shift of the location of the wind–SST

✉ Zeng-Zhen Hu  
Zeng-Zhen.Hu@NOAA.GOV

<sup>1</sup> School of Earth Sciences, Zhejiang University,  
Hangzhou 310027, Zhejiang, China

<sup>2</sup> Climate Prediction Center, NCEP/NWS, NOAA 5830  
University Research Court, College Park, MD 20740, USA

interaction region. According to An and Wang (2000), zonal location shift of the atmosphere–ocean coupling affects ENSO frequency through zonal advection feedback that changes the period and growth of coupled instability.

On the basis of knowing the westward shift of the tropical Pacific climate variability since 1999/2000 (e.g., Hu et al. 2017a, b), this work focuses on possible factors leading to the shift. These factors include Kelvin wave activity, low-level wind, and zonal gradient across the equatorial Pacific. The spatial change of the tropical Pacific climate variability after 2000 is first examined, through analyzing the variabilities of SST, deep convection, and ocean thermocline depth anomalies. We then discuss the possible association of the spatial change of the variabilities with oceanic Kelvin wave activity, surface westerly/easterly wind, the heat budget of the oceanic mixed-layer, and zonal gradient of climate across the tropical Pacific, as well as the possible influence of the spatial change of tropical Pacific climate variability on the extra-tropics. The data used in the analysis are described in Sect. 2; Sect. 3 presents the results. A summary and some discussion are given in Sect. 4.

## 2 Data and methods

The ocean dataset analyzed in this work is from the Global Ocean Data Assimilation System (GODAS, Behringer 2007). Ocean temperature and the depth of 20 °C isotherm (D20) from GODAS are analyzed. Using data from GODAS, the oceanic Kelvin wave index was calculated. The oceanic Kelvin wave index is defined as standardized projections of GODAS pentad (5-day) mean ocean temperature anomalies (OTAs) onto the first mode of an extended empirical orthogonal function (eEOF) that is computed using OTAs of the upper 300 meters along the equator between 135.5°E–94.5°W for each 14 contiguous pentad (5-days) means (Seo and Xue 2005). There are total 14 patterns in 1st eEOF mode, which represent 14 contiguous pentads and approximate the propagation of the Kelvin wave. The projections onto each of the 14 patterns are assigned to the longitude location of that pattern's longitude with maximum loading. The eEOF pattern can be found at [http://origin.cpc.ncep.noaa.gov/products/GODAS/ocean\\_briefing\\_new/eeve\\_1.gif](http://origin.cpc.ncep.noaa.gov/products/GODAS/ocean_briefing_new/eeve_1.gif). The oceanic Kelvin wave index is routinely monitored at NOAA Climate Prediction Center ([http://www.cpc.ncep.noaa.gov/products/people/yxue/ocean\\_briefing\\_new/OKV\\_index.gif](http://www.cpc.ncep.noaa.gov/products/people/yxue/ocean_briefing_new/OKV_index.gif)).

According to Huang et al. (2010), the tendency of monthly mean temperature of the ocean mixed layer is defined as:

$$\frac{\partial T}{\partial t} = Q_u + Q_v + Q_w + Q_{zz} + Q_q + R \quad (1)$$

where  $\partial T/\partial t$  is the tendency of the mixed layer ocean temperature.  $Q_u$ ,  $Q_v$ ,  $Q_w$ ,  $Q_{zz}$ , and  $Q_q$  are zonal advection, meridional advection, vertical entrainment, vertical diffusion, and adjusted surface heat flux, respectively (Huang et al. 2010). The residual term  $R$  represents the effect of horizontal heat diffusion and the contributions of sub-monthly processes, such as diurnal variations and tropical instability waves (Huang et al. 2010). The heat budget of the ocean mixed layer is calculated based on the GODAS data (Huang et al. 2010).

To examine the strength of atmosphere–ocean coupling, the regression of monthly mean zonal wind stress anomalies onto the Niño3 index is computed, and then used to measure the surface wind-SST interaction (Li et al. 2019), which is also called Bjerknes feedback by Lloyd et al. (2009) or atmospheric Bjerknes feedback by Bellenger et al. (2014). The Niño3 index is the average of SSTA in (5°S–5°N, 150°W–90°W). Monthly mean zonal wind stress at the surface and 6 hourly mean zonal wind at 1000 hPa are from the NCEP–DOE reanalysis on 1° longitude by 1° latitude grid (Kanamitsu et al. 2002). Monthly mean outgoing long-wave radiation (OLR) data on a 2.5° longitude × 2.5° latitude grid from Liebmann and Smith (1996) and SST on a 2° longitude × 2° latitude grid of ERSST version 5 (ERSSTv5) from Huang et al. (2017) are also analyzed. OLR is used as a proxy for deep convective activity over the tropical oceans. All the data used in this work are from January 1979 to December 2017. The referred monthly climatologies were calculated using data in January 1979–December 2017.

## 3 Results

### 3.1 Evidence of spatial change of variability

Consistent with previous work (McPhaden 2012; Hu et al. 2012, 2013, 2016, 2017a), Fig. 1a shows that SSTA variability in the eastern equatorial Pacific is weaker during 2000–2017 compared with that during 1979–1999. The maximum center of SSTA variability is near the South American coast in 1979–1999 (bars in Fig. 1a), while it is a broad peak spanning much of the central-eastern Pacific in 2000–2017 (line in Fig. 1a). The (relative) peak around 90°W in both periods might be associated with the large variability of strong upwelling over the region (<https://www.njweather.org/content/what-weak-la-ni%C3%B1a-event-might-have-store-new-jersey-winter>; see Fig. 1 for the longitude zone of equatorial upwelling). The notable variability of upwelling may be related to the fact that there are multiple islands in this region. The significance of the change of the variance at each longitude grid is assessed based on 1000 Monte-Carlo resamples; significance is shown at the 95% level, using the  $F$ -test. The variance is slightly increased in

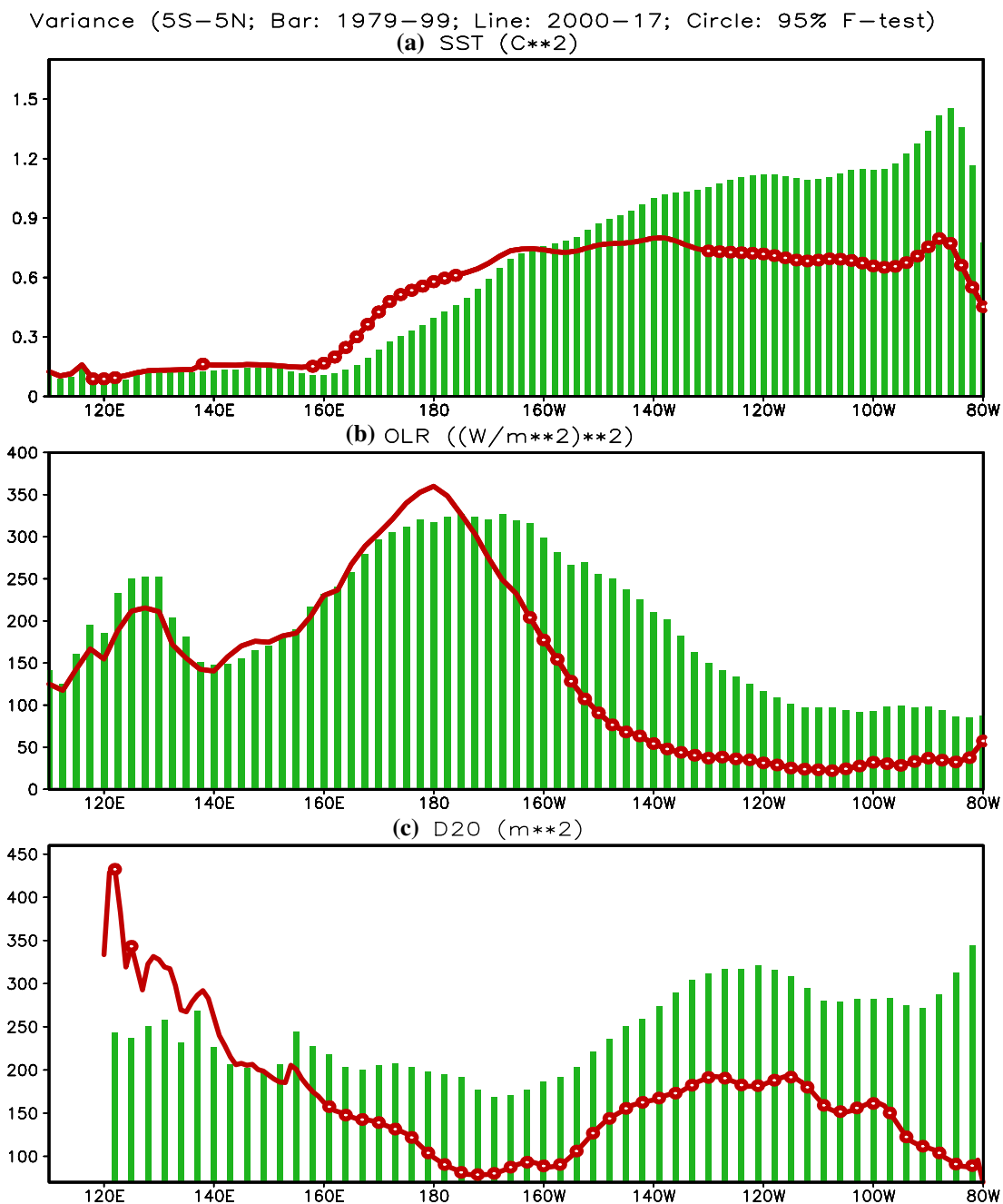


**Fig. 1** Longitude-dependent variance of monthly mean **a** SSTA, **b** OLR, and **c** D20 anomalies averaged in 5°S–5°N in January 1979–December 1999 (bar) and in January 2000–December 2017 (curve). The units are (°C)<sup>2</sup>, (w/m<sup>2</sup>)<sup>2</sup>, and m<sup>2</sup>, respectively. The curve with

circles indicates when the change of the variance is significant at the 95% significance level using an *F*-test based on 1000 Monte-Carlo resamples

160°E–170°W and significantly reduced in 130°W–80°W, indicating a westward shift of the maximum variability of SSTA or suppression of the variability in the eastern Pacific.

Consistently, the variability of equatorial deep convection, represented by OLR variance, is also displaced westward and reduced in the eastern Pacific, due to the statistically significant suppression of deep convection

(OLR variability) in the eastern Pacific (160°–80°W; Fig. 1b). For D20 anomaly (Fig. 1c), in addition to significant decrease of the variability in the eastern Pacific, similar to that of SST and OLR (Fig. 1a, b), its variability also significantly decreases in the central Pacific (Fig. 1c). The variability decrease of D20 anomaly in the central and eastern equatorial Pacific may be associated with

suppression of Kelvin wave activity. That will be discussed in next subsection.

The westward shifts of the variability of these individual fields/variables collectively suggest an overall westward shift of the whole atmosphere–ocean climate system in the tropical Pacific. This is also consistent with spatial changes of the wind–SST interaction from 1979–1999 to 2000–2017 (Fig. 2). Compared to the earlier period (Fig. 2a), the positive wind–SST interaction in the western and central tropical

and northwestern Pacific strengthens, while the negative feedback strengthens as well in the southeastern Pacific during 2000–2017 (Fig. 2b, c). The enhanced interaction in the western and central tropical Pacific is consistent with the enhanced variability of SSTA along the equator in 155°E–175°W shown in Fig. 1a. Such changes in the regression patterns mean a northwestward shift of the atmosphere–ocean coupling (Hu et al. 2017b). This westward shift matches the post–1999/2000 tendency toward

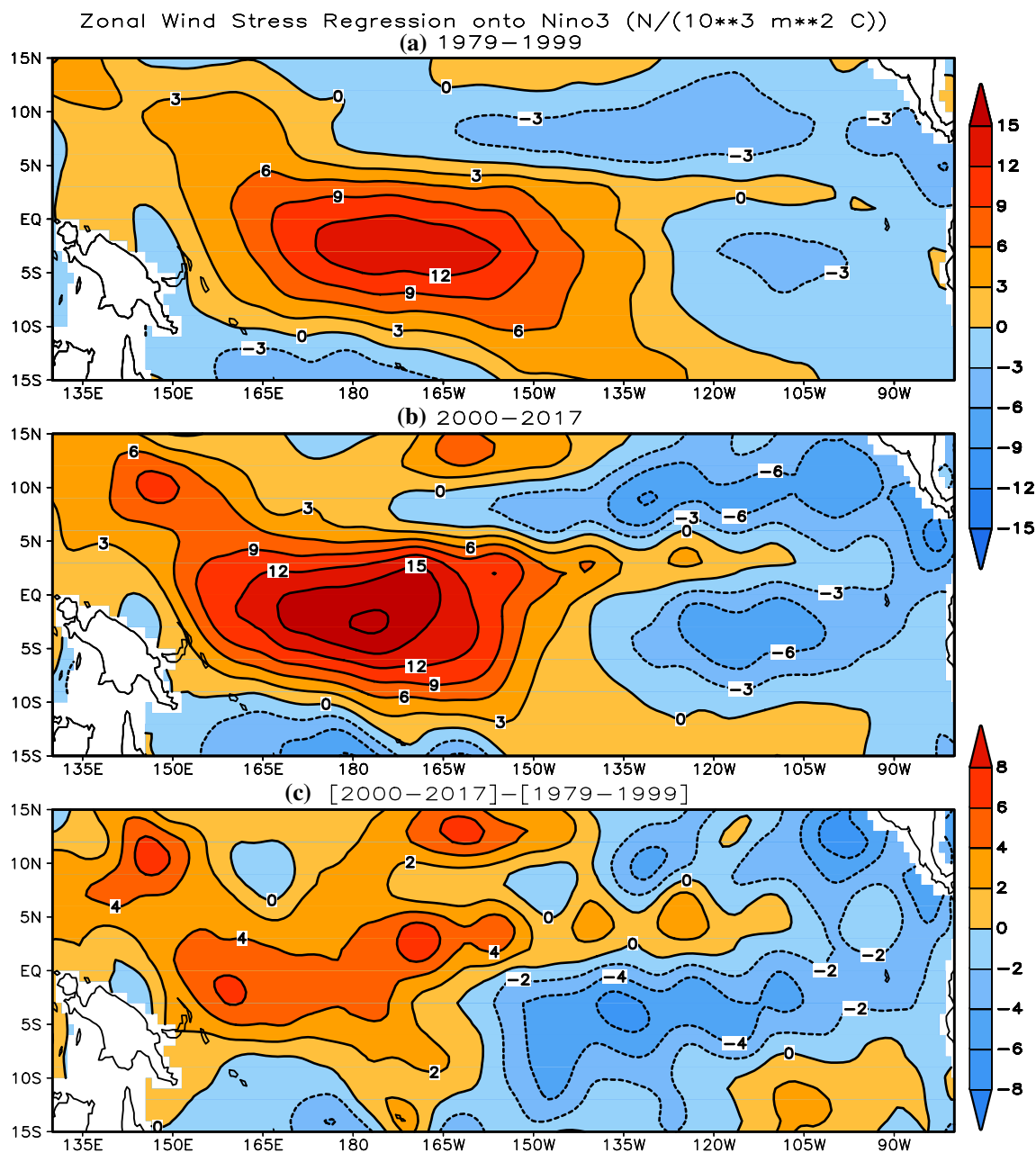


**Fig. 2** Simultaneous regressions of zonal wind stress anomalies onto the Niño3 index in **a** January 1979–December 1999, and **b** January 2000–December 2017, which was referred to as the wind–SST inter-

action. **c** Difference of **b** and **a**. The unit is  $N/(10^3 m^2 C)$  and the contour interval is 3 in **a**, **b**, and 2 in **c**

more CP vs EP El Niño events (Yeh et al. 2009; Yu et al. 2011; McPhaden 2012; Horii et al. 2012). In addition, both the maxima of mean wind-SST interaction and the change (Fig. 2) present in 2–3°S instead of at the equator may suggest that some other feedbacks (such as the wind-evaporation-SST feedback; Xie and Philander 1994) may also play a role to some extent.

### 3.2 Possible factors associated with spatial change of the variability

Earlier work has suggested that the variability suppression of SST, OLR and D20 anomalies in the eastern tropical Pacific after 2000 is affected by the enhancement of the west-east contrast of the mean state across the tropical Pacific (e.g., Hu et al. 2013). Nevertheless, the factors resulting in the zonal migration of the variability are ambiguous. It is speculated here that the zonal migration may be associated with the statistical feature change of some high-frequency variability as well as the mean state change.

One of these associated high-frequency variabilities is oceanic Kelvin wave activity along the equator. Here, the oceanic Kelvin wave is measured by the standardized projections of GODAS pentad mean OTAs onto the first mode of eEOF of OTAs for each of 14 contiguous pentad means along the equator. Through calculating variances of the projection at different longitudes and its temporal evolution averaged in 1979–1999 and 2000–2017, respectively, the intensity and propagation of oceanic Kelvin waves and their differences can be identified. It is noted that the mean variance of the oceanic Kelvin wave has clear seasonality: large in cold months and small in warm months of Northern Hemisphere (contours in Fig. 3b, for mean in 1979–1999). Moreover, it varies with longitude. That might be suggested that the method used to isolate oceanic Kelvin wave captures not pure oceanic Kelvin wave.

Compared to the relatively constant intensity of oceanic Kelvin wave activity in the central and eastern equatorial Pacific during 1979–1999 (bars in Fig. 3a), the overall intensity weakens during 2000–2017 (line in Fig. 3a), in agreement with an overall weakening of tropical Pacific climate variability (Hu et al. 2013, 2016, 2017a). Furthermore, the reduction of oceanic Kelvin wave variance shows a longitudinal dependence during 2000–2017. The reduction during the later period is most remarkable in the 175°–145°W and 120°–110°W regions (significant at 95% level), and less pronounced in 165°E–175°E and 135°–125°W (Fig. 3a). Such longitude-dependent reduction of Kelvin wave variance shown in Fig. 3a seems mainly occurred in boreal winter, the peak phase of ENSO (shading in Fig. 3b). The possible reasons leading to the longitude dependence deserve further investigation. During the other months, the overall reduction may imply a weakening of Kelvin wave activity during the

initiate and development phases of ENSO. The significant weakening of oceanic Kelvin wave activity in the central and eastern equatorial Pacific (175°–145°W) may suggest that zonal transport of oceanic heat from the warm pool in the western tropical Pacific to the central and eastern equatorial Pacific via oceanic Kelvin waves (Kessler et al. 1995) decreased, leading to a westward shift of the ENSO-associated atmosphere–ocean variability in the equatorial Pacific.

The change of the oceanic Kelvin wave activity is associated with a change in the low-level winds. The suppression of oceanic Kelvin wave activity in the longitude belt of 175°–145°W during 2000–2017 compared with that during 1979–1999 (Fig. 3a) coincides with a weakening of average intensity (or reduction of frequency) of the low-level westerly winds in 170°–140°W (Fig. 4a) and a westward shift of the low-level easterly winds in the central and eastern Pacific (Fig. 4b). Hu and Fedorov (2016) (see their Fig. 1) noted that total westerly wind is a good approximation of westerly wind anomaly and a good measurement for westerly wind bursts. Hu et al. (2012) found that stronger and more eastward extended westerly winds along the equatorial Pacific in the early months of a year is associated with active atmosphere–ocean interaction over the cold tongue/the Intertropical Convergence Zone (ITCZ) complex, as well as a more intense oceanic thermocline feedback, favoring EP El Niño development, while weaker and more westward confined westerly winds along the equatorial Pacific in the early months of a year is associated with suppressed atmosphere–ocean interaction over the cold tongue/the ITCZ complex, as well as less intense oceanic thermocline feedback, favoring CP El Niño development. Chen et al. (2015) argued that the asymmetry, irregularity and extremes of El Niño may result from variations in westerly wind bursts, and properly accounting for the interplay between the canonical cycle and westerly wind bursts may improve El Niño prediction.

The westward shift of the atmosphere and ocean interaction of tropical Pacific climate variability and change of the oceanic Kelvin wave activity are also consistent with the change of the heat budget of the oceanic mixed-layer. For example, compared with 1979–1999 (contours in Fig. 5), the variability of both vertical entrainment ( $Q_w$ ), vertical diffusion ( $Q_{zz}$ ), and adjusted surface heat flux ( $Q_q$ ), decrease in the eastern Pacific (140°W–105°W), in addition to some increase in the far eastern Pacific and near the South American coast (105°W–85°W) after 2000 (shading in Fig. 5). The decrease is especially obvious for vertical entrainment and vertical diffusion, as well as the adjusted surface heat flux, in 140°–110°W (Fig. 5c, d), while the increase in variability is evident in the zonal and meridional advection from 110°W eastward to the coast (Fig. 5a, b). That might be associated with variation of coastal El Niño (Hu et al. 2019). The suppression of the variability of the vertical entrainment and vertical diffusion in 140°–110°W (Fig. 5c) is downstream

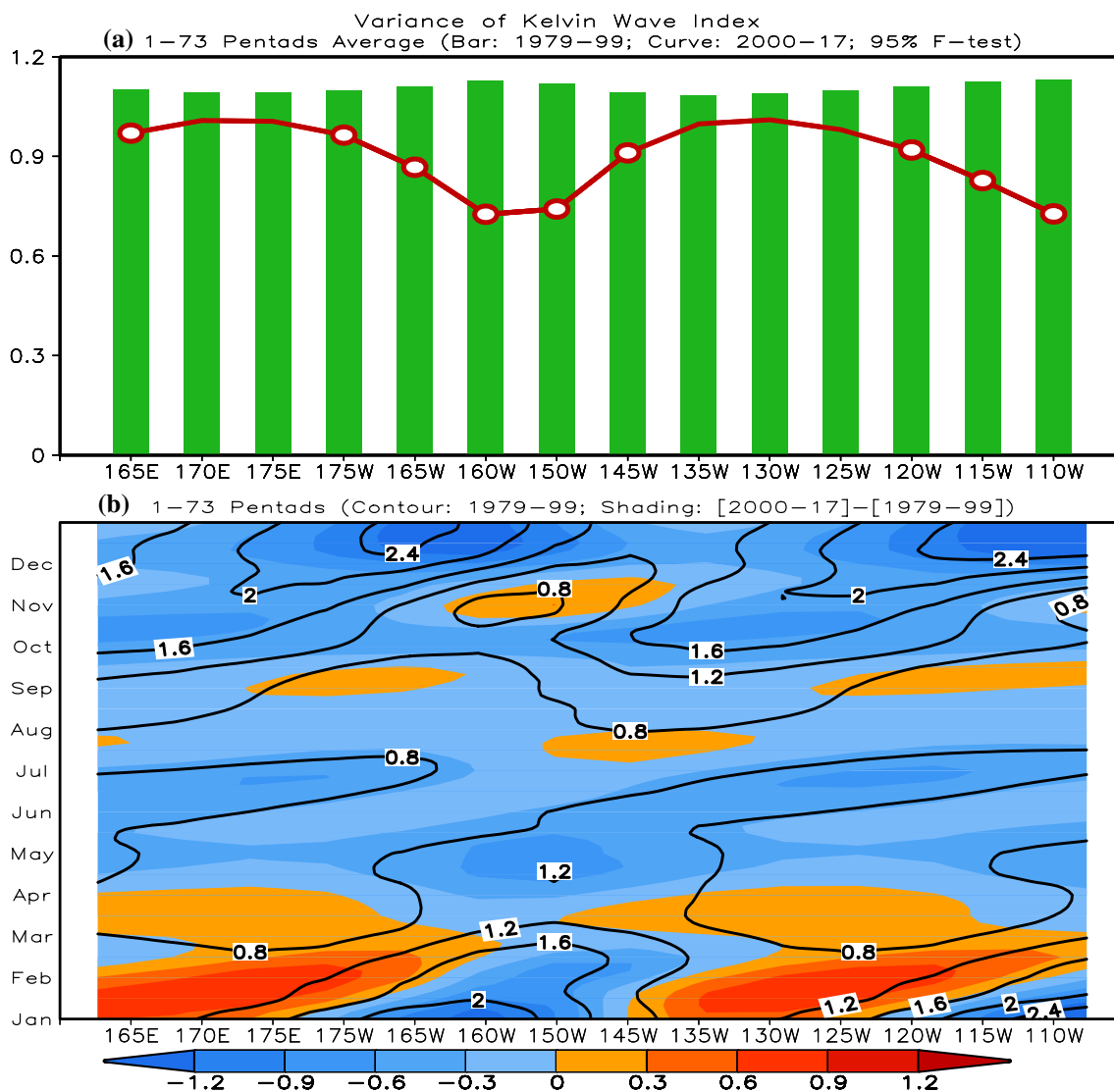


**Fig. 3 a** Longitude-dependent variance of pentad oceanic Kelvin wave index averaged in January 1979–December 1999 (bars) and in January 2000–December 2017 (curve). The curve with circles indicates when the change of the variance is significant at the 95% significance level, using an *F*-test based on 1000 Monte-Carlo resamples. **b**

Longitude- and pentad-dependent variance of pentad oceanic Kelvin wave index averaged in January 1979–December 1999 (contours) and the differences between the means averaged in January 2000–December 2017 and in January 2000–December 2017 (shading). The contour interval is 0.4 and shading interval is 0.3

of the decline of westerly wind (Fig. 4a). Also, the variance changes for all the terms are much smaller in the central and western Pacific than in the eastern Pacific. All these results are generally consistent with Guan and McPhaden (2016). They noted that the thermocline feedbacks weakened from 1980 to 1999 and into the 2000s, while the zonal advective feedbacks were less affected. The thermal damping weakened after 2000, particularly in the Niño3 region.

In addition to its impact on the intensity of the variability, the zonal contrast of the mean state may also be associated with the westward shift of atmosphere–ocean variability in the tropical Pacific. Following Yang et al. (2016), the zonal gradient index is defined as the difference between mean

SSTA in the western (5°S–5°N, 145°–165°E) and eastern (5°S–5°N, 120°–120°W) tropical Pacific (see the rectangles in Fig. 6b, c), which are associated with the warm pool and cold tongue regions, respectively (Fig. 6b). Statistically, the zonal gradient index and Niño3.4 indices have significantly negative correlations (-0.82, Fig. 6a).

It is noted that the zonal location shift of 28 °C isothermal contour between the two periods is not so obvious (Fig. 6c), nevertheless the increase of mean zonal gradient of SST is evident since 2000 (Hu et al. 2013, 2017a) (Fig. 6b, c). To check the statistical connection of zonal location of maximum SSTA with zonal gradient, we extend the data back to 1854 by using ERSSTv5. From Fig. 7, it is seen

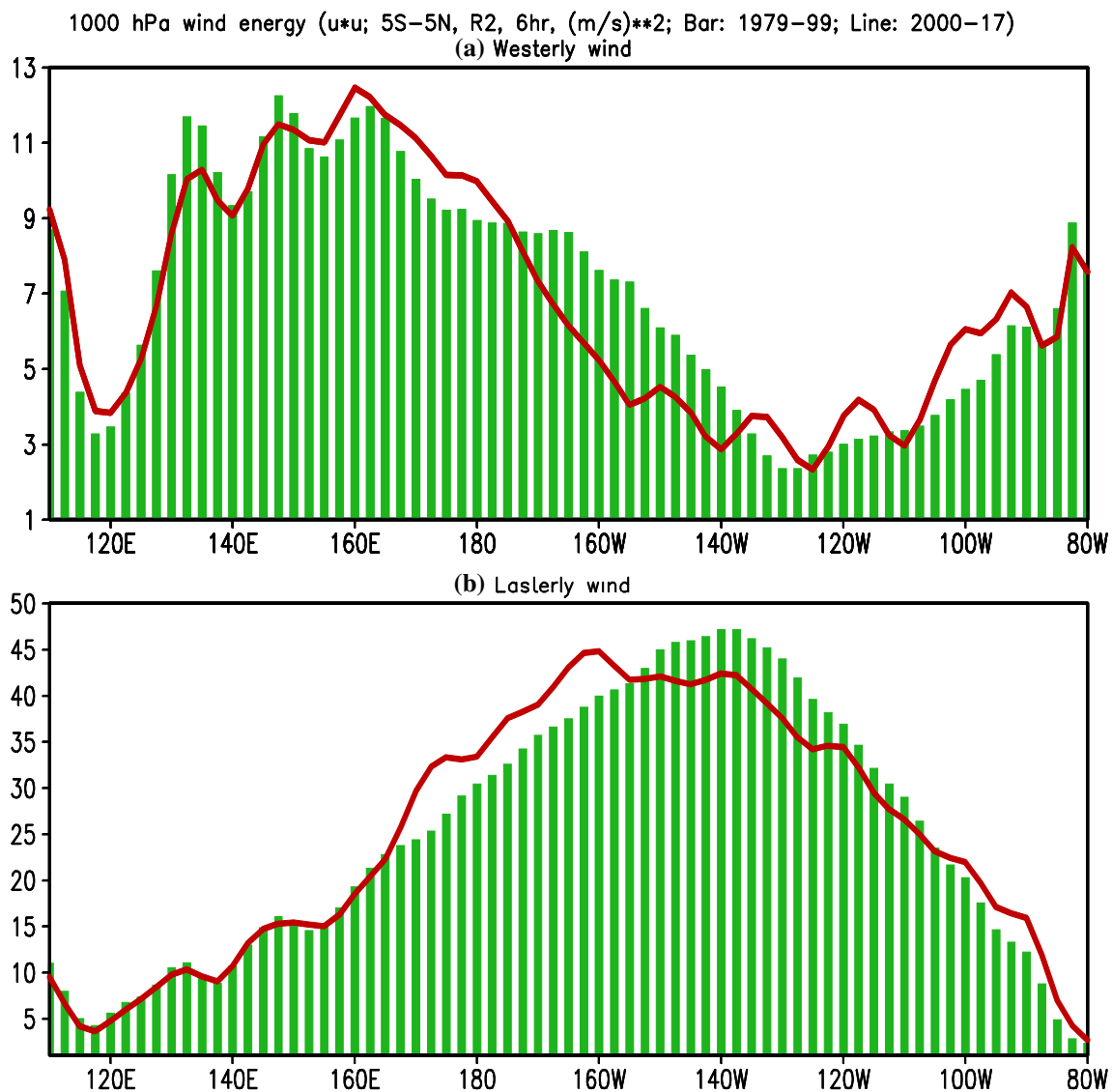


**Fig. 4** Longitude-dependent total **a** westerly wind ( $u > 0.0$ ) and **b** easterly wind ( $u < 0.0$ ) energy (referred to as  $u^2$ ) averaged in  $5^{\circ}\text{S}$ – $5^{\circ}\text{N}$  in January 1979–December 1999 (bar) and in January 2000–December

2017 (curve). The zonal wind refers to the 6 hourly mean zonal wind at 1000 hPa. The unit is  $(\text{m/s})^2$

that maximum positive SSTA (red circles) is more likely present westward when the gradient increases, and maximum negative SSTA (green triangles) is more likely present eastward when the gradient increases. This link maintains both before and after 1978/79 (Fig. 7). Comparing January 1979–December 1999 (Fig. 7a) with January 2000–December 2017 (Fig. 7b), the overall location of maximum SSTA seems further westward in the later period than in the earlier period. Furthermore, the connection of the zonal gradient of SSTA with the longitude of maximum positive/negative SSTA on the equatorial Pacific is more robust for larger amplitudes of SSTA in the Niño3.4 region (for example, absolute value of Niño3.4 SSTA  $> 0.5^{\circ}\text{C}$ ; Fig. 8). This

means that the zonal gradient of SSTA across the tropical Pacific might be partially affected by ENSO evolution.

### 3.3 Impact of spatial change of the tropical Pacific variability on the extratropics

The westward shift of atmosphere–ocean variability in the tropical Pacific Ocean may modulate the teleconnection from the tropical Pacific to the extratropics, and hence may impact the predictability and prediction skill of extra-tropical climate. Following Jin and Hoskins (1995), here we use the zonal departure of the meridional component of wind at 200 hPa ( $v_{200}$ ) to track the forced teleconnection from the tropical Pacific. From Fig. 9, it is seen that when the

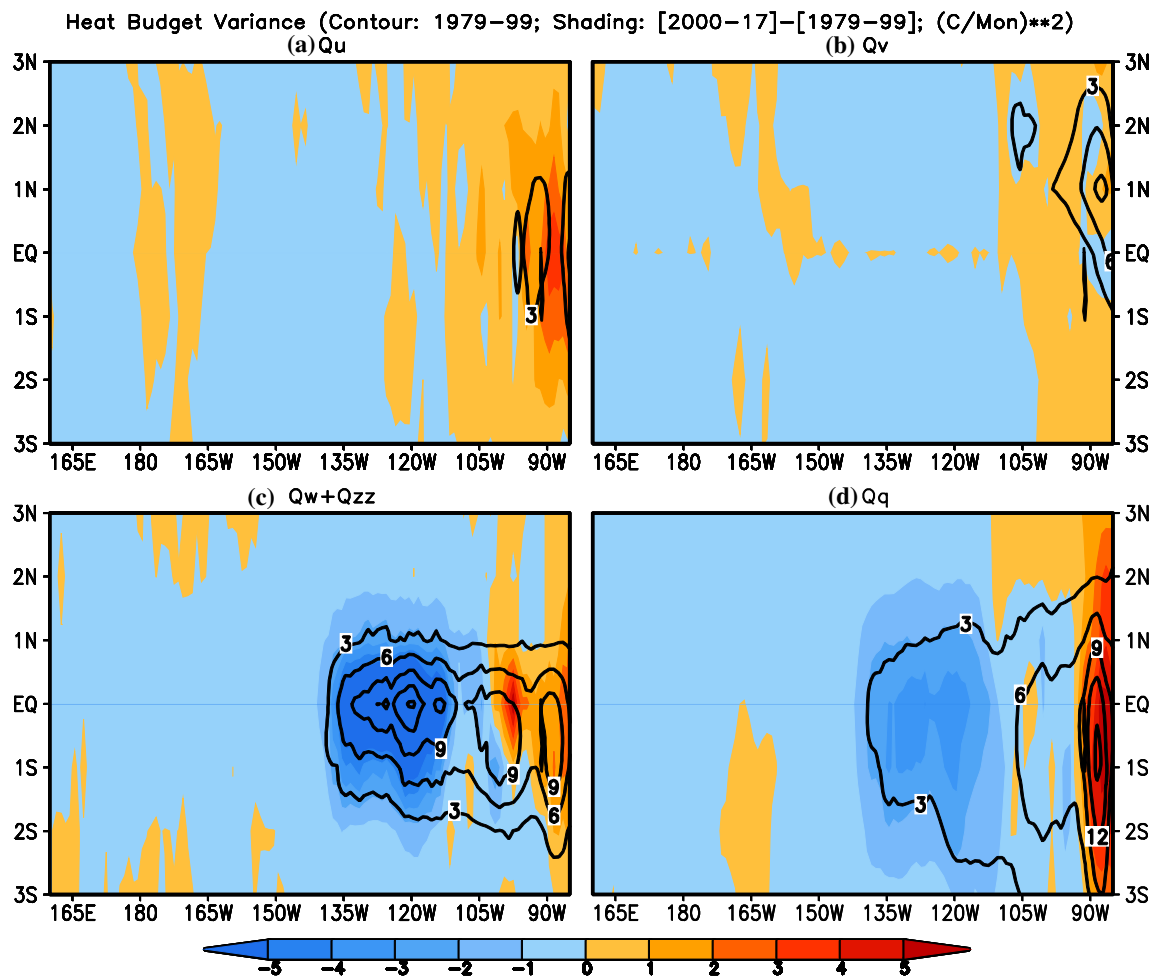


**Fig. 5** Variance of mixed-layer heat budget terms in 1979–1999 (contour) and the difference of 2000–2017 minus 1979–1999 (shading) for **a** zonal advection ( $Q_u$ ), **b** meridional advection ( $Q_v$ ), **c** vertical

entrainment ( $Q_w$ ) and vertical diffusion ( $Q_{zz}$ ), and **d** adjusted surface heat flux ( $Q_q$ ). The unit is  $(^{\circ}\text{C}/\text{Month})^2$

atmosphere–ocean coupling shifts westward (represented by OLR in  $(5^{\circ}\text{S}–5^{\circ}\text{N}, 165^{\circ}\text{E}–165^{\circ}\text{W})$ ; see the rectangles in Figs. 2b, 9b, and the contour in Fig. 9b), the tropical centers of the forced teleconnection patterns shift westward, compared to the coupling located in the central and eastern equatorial Pacific (represented by OLR in  $(5^{\circ}\text{S}–5^{\circ}\text{N}, 175^{\circ}\text{E}–155^{\circ}\text{W})$ ; see the rectangles in Figs. 2a, 9a, and the contour in Fig. 9a).

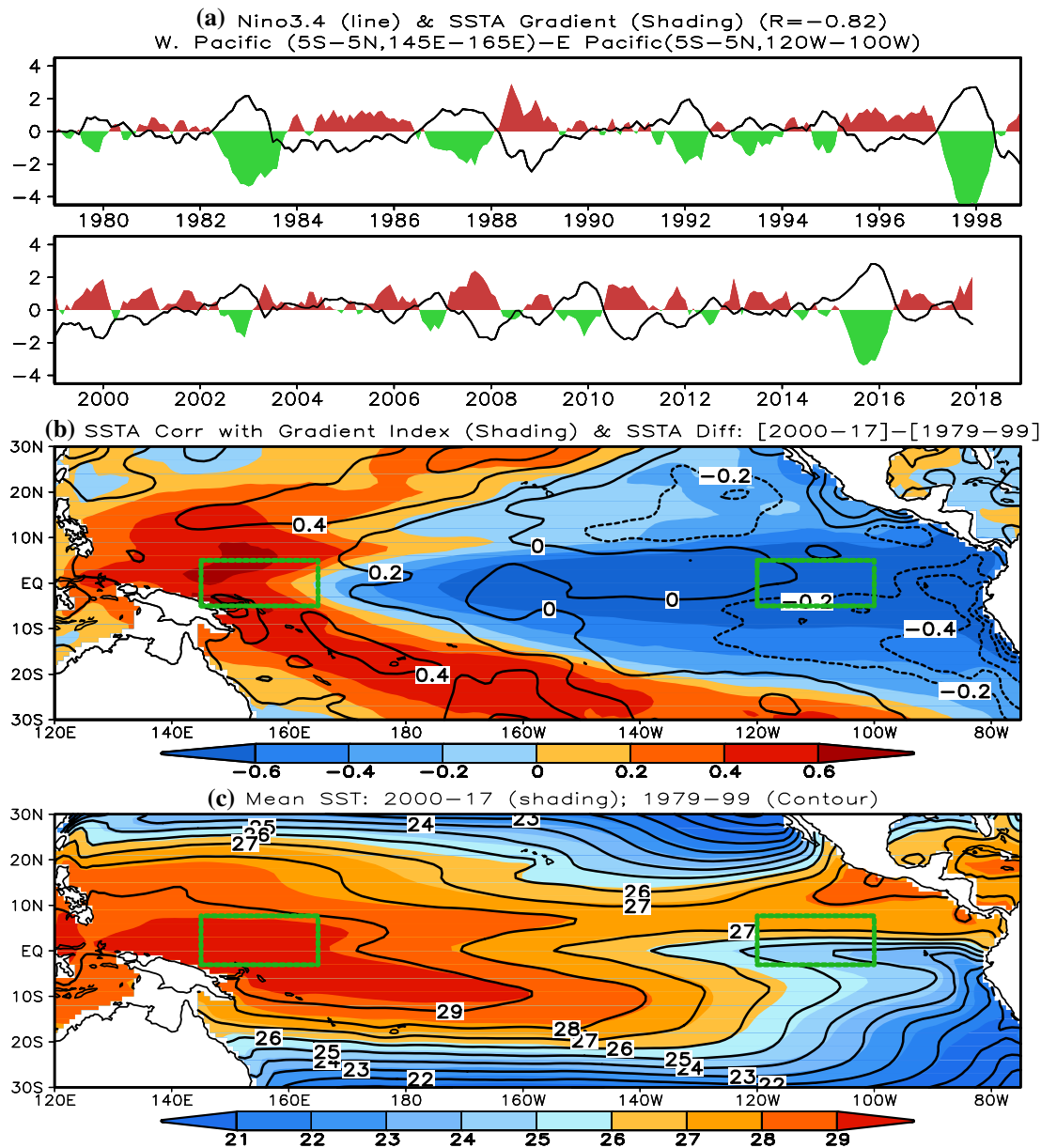
For correlations in the extratropics, some changes are also visible. For example, over the United States, the region of significant negative correlation shifts from the northwest to the southeast (Fig. 9). These changes may imply a pattern change of ENSO impacts on extratropical regions due to the westward shift of atmosphere–ocean coupling in the tropical Pacific. That is also consistent with the distinctive impact of the CP and EP El Niño on the extratropics (Hu et al. 2012; Garfinkel et al. 2013), and with well documented sensitivity

of extratropical response to zonal location of the equatorial forcing (e.g., Ting and Sardeshmukh 1993).

## 4 Summary and discussion

In this work, we investigate the westward shift of atmosphere–ocean coupling in the tropical Pacific since 2000. In addition to a weakening of climate variability in the eastern tropical Pacific, profound westward shifts in the variability of SST, deep convection, and D20 are observed during 2000–2017 when compared to that during 1979–1999. The westward shift of the climate variability in the tropical Pacific is also seen in the change of the wind–SST interaction from 1979–1999 to 2000–2017. Compared with the earlier period, the atmosphere–ocean coupling is shifted northwestward during the later period.





/cpc/home/hzz/CPChu/WestShift/40\_SST\_gradient01\_scr

**Fig. 6** **a** The Nino3.4 (line) and zonal gradient (shading) indices in January 1979–December 2017. The zonal gradient index is defined as the difference of averaged SSTAs between the western (5°S–5°N, 145°–165°E) and eastern (5°S–5°N, 120°–10°W) tropical Pacific [see the green rectangles in **b**, **c**, following Yang et al. (2016)]. The cor-

relation between the two indices is  $-0.82$ . **b** Correlations of SSTAs with the gradient index in January 1979–December 2017. **c** is the mean of SST in January 1981–December 2010 (contour), and differences of SST between January 2000–December 2017 and January 1979–December 1999 (shading) (unit: °C)

Such westward shifts of variability are associated with a change in oceanic Kelvin wave activity along the equator. In addition to the overall weakening, the post-2000 reduction of oceanic Kelvin wave variance is most pronounced in the region of 175°–145°W and 120°–110°W. The suppression of oceanic Kelvin wave activity in 175°–145°W coincides with a weakening of the low-level westerly winds in the same longitude belt and a westward shift of the low-level easterly winds in the central

and eastern tropical Pacific. Furthermore, the westward shift of the atmosphere–ocean interaction of the tropical Pacific is seen in the heat budget of the oceanic mixed-layer. Compared to 1979–1999, the variability of both the dynamical (vertical entrainment and vertical diffusion) and thermodynamical terms decrease in the eastern Pacific in 2000–2017. The reduction in variability is more evident in the vertical entrainment and vertical diffusion, as well as the adjusted surface heat flux, in the longitude band

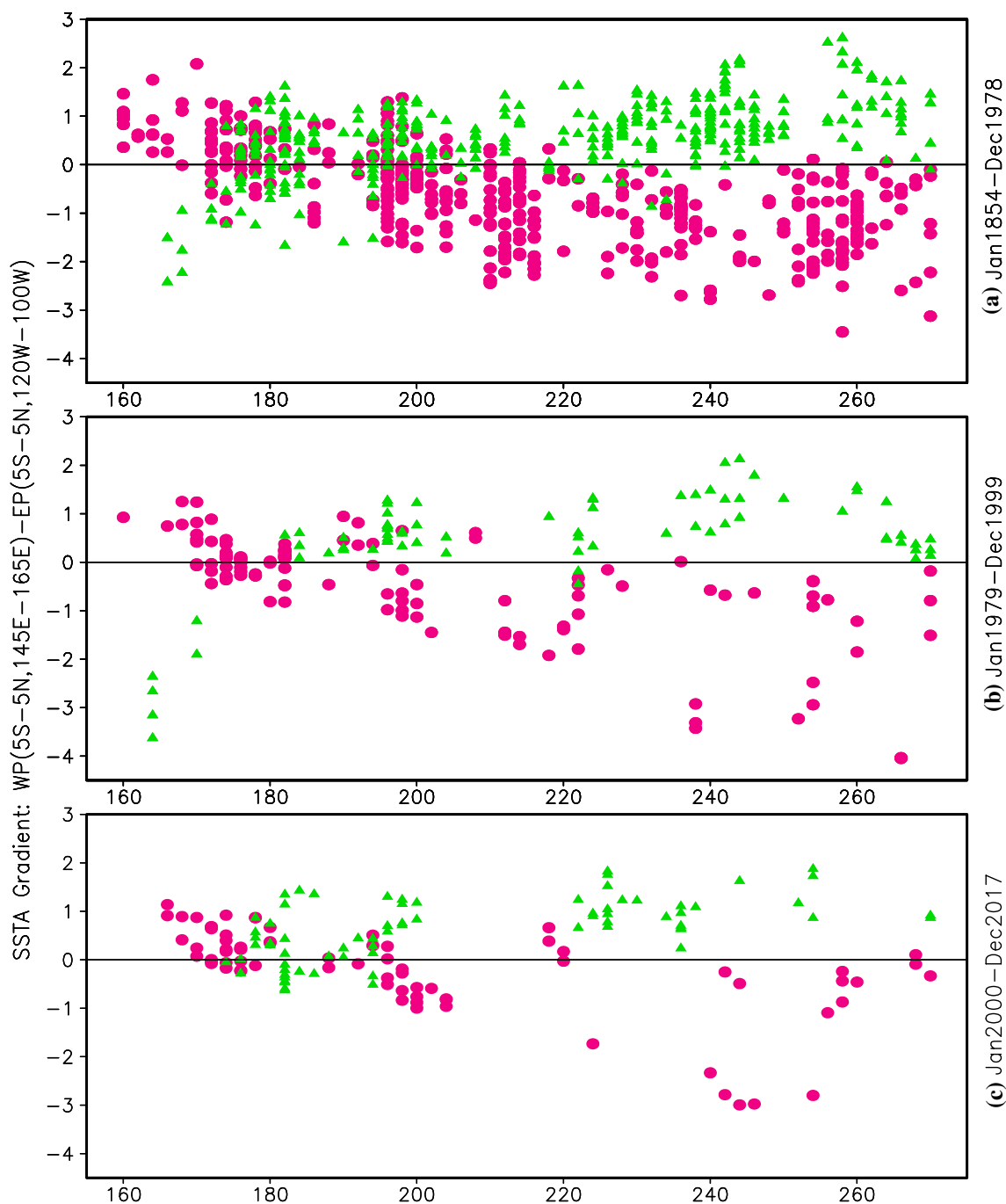


**Fig. 7** Scatter of the zonal gradient index (y-axis) and the longitude location of maximum positive (red dot) and negative (green triangle) SSTA between 160°E and 90°W along the equator in **a** Janu-

ary 1854–December 1978, **b** January 1979–December 1999, and **c** January 2000–December 2017

140°–110°W, which is in the downstream of the weakening of the low-level westerly winds. The westward shift of the atmosphere–ocean coupling in the tropical Pacific may be also associated with an interdecadal change of the mean state in the tropical Pacific (L’Heureux et al. 2013). With observed enhancement of zonal contrast of the mean state across the tropical Pacific, the location of

maximum positive SSTA on the equator is more likely shifted westward.

The connection of the westward shift of the atmosphere–ocean coupling in the tropical Pacific with an interdecadal change of the mean state in the tropical Pacific is consistent with previous work. For example, Bunge and Clarke (2014) argued that both pre-1973 and post-1998

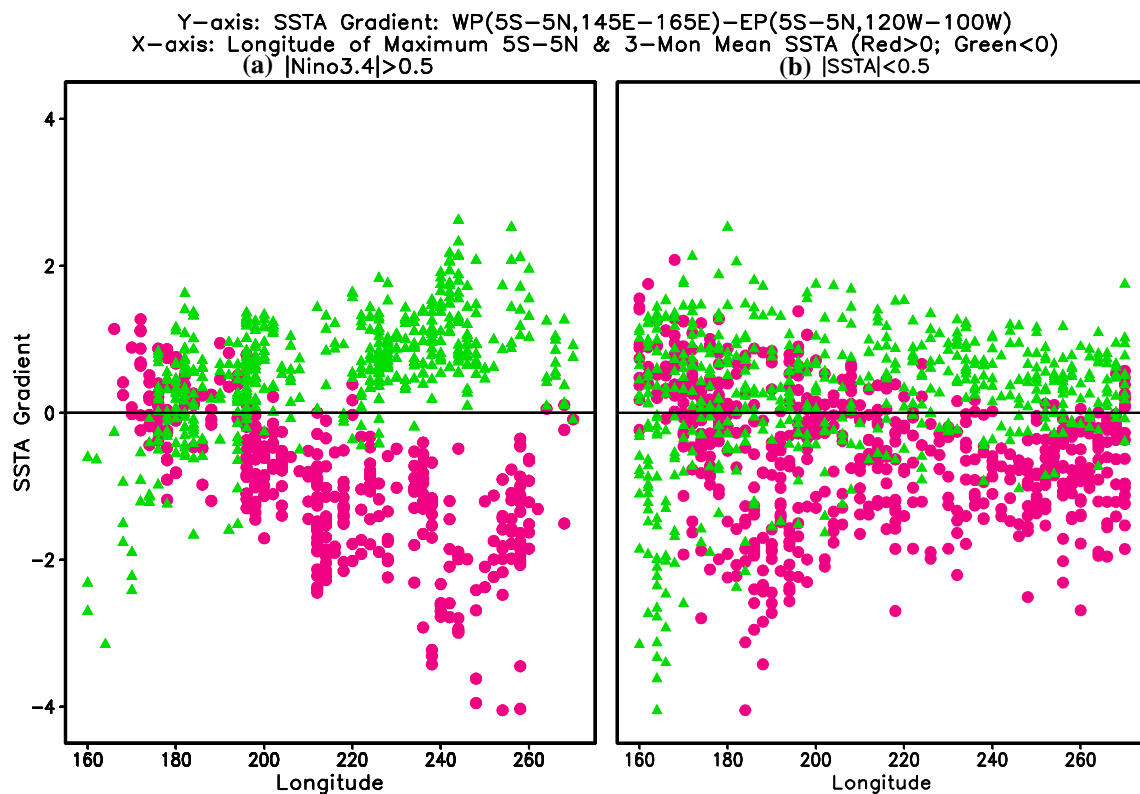


**Fig. 8** Scatter of the zonal gradient index (y-axis) and the longitude location of maximum positive (red dot) and negative (green triangle) SSTA between 160°E and 90°W along the equator (x-axis) in January 1854–December 2017 for **a**  $|Ni\tilde{u}o3.4| \geq 0.5$  °C and **b**  $|SSTA| < 0.5$  °C

periods were characterized by mean La Niña-like conditions, including a westward displacement of the associated anomalous wind forcing. As a result, the canonical (EP) El Niño can't fully develop in the eastern Pacific, and thus the ENSO-related tropical Pacific variability decreases. Hu et al. (2012) noted that, compared with CP El Niño, EP El Niño is associated with stronger and more eastward-extend westerly wind anomalies along the equatorial Pacific in the first half of the year (January–July), as well as stronger atmosphere–ocean interaction over the cold tongue/the Intertropical Convergence Zone complex and more intensive oceanic thermocline feedback. This agrees with the change of oceanic Kelvin wave activity and energy budget of the oceanic mixed-layer after 2000 discussed in this work. Recently, Hu and Fedorov (2018) argued that cross-equatorial southerly wind trends in the eastern tropical Pacific, which seems associated with a Pacific Meridional Mode-like (Chiang and Vimont 2004) or North Pacific mode-like (Peng et al. 2018) SSTA pattern in the eastern tropical Pacific and warming in the tropical North Atlantic Ocean, are a potential factor to suppress the ENSO variability and to force the atmosphere–ocean coupling region in the tropical Pacific moving westward mainly through ocean dynamical processes.

An and Wang (2000) demonstrated that the westward (eastward) shift of the atmosphere–ocean coupling

(or westerly wind stress anomaly) leads to an increase (a decrease) in ENSO frequency, and a reduction (an enhancement) in the amplitude of ENSO events. This is consistent with observational evidence since 2000 (McPhaden 2012; Horii et al. 2012; Hu et al. 2012, 2013, 2016, 2017a, b; Xiang et al. 2013; Kumar and Hu 2014; Bunge and Clarke 2014; Lübbecke and McPhaden 2014). Also, the westward shift of the atmosphere–ocean coupling in the tropical Pacific may be a major reason leading to the shortening of the periods of WWV and Niño3.4 indices, as well as the reduction in the lead time of WWV to ENSO (Niño3.4 index) (McPhaden 2012; Kumar and Hu 2014; Hu et al. 2017b). Likely as a result, ENSO prediction skill has decreased since 1999/2000 (Wang et al. 2010; Barnston et al. 2012). Nevertheless, it is unclear for the impact of strength change of atmosphere–ocean coupling processes, such as zonal advection and thermocline feedbacks, on ENSO frequency.

The mean state and ENSO feature (such as spatial pattern and frequency) changes may be associated with the tropical signature of global warming (e.g., Capotondi et al. 2015; Wang et al. 2016). For example, Collins et al. (2010) argued that in a global warming scenario the tropical easterly trade winds are expected to weaken, and zonal SST gradients across the Pacific are expected to become smaller. Such a mean state change might be a crucial factor

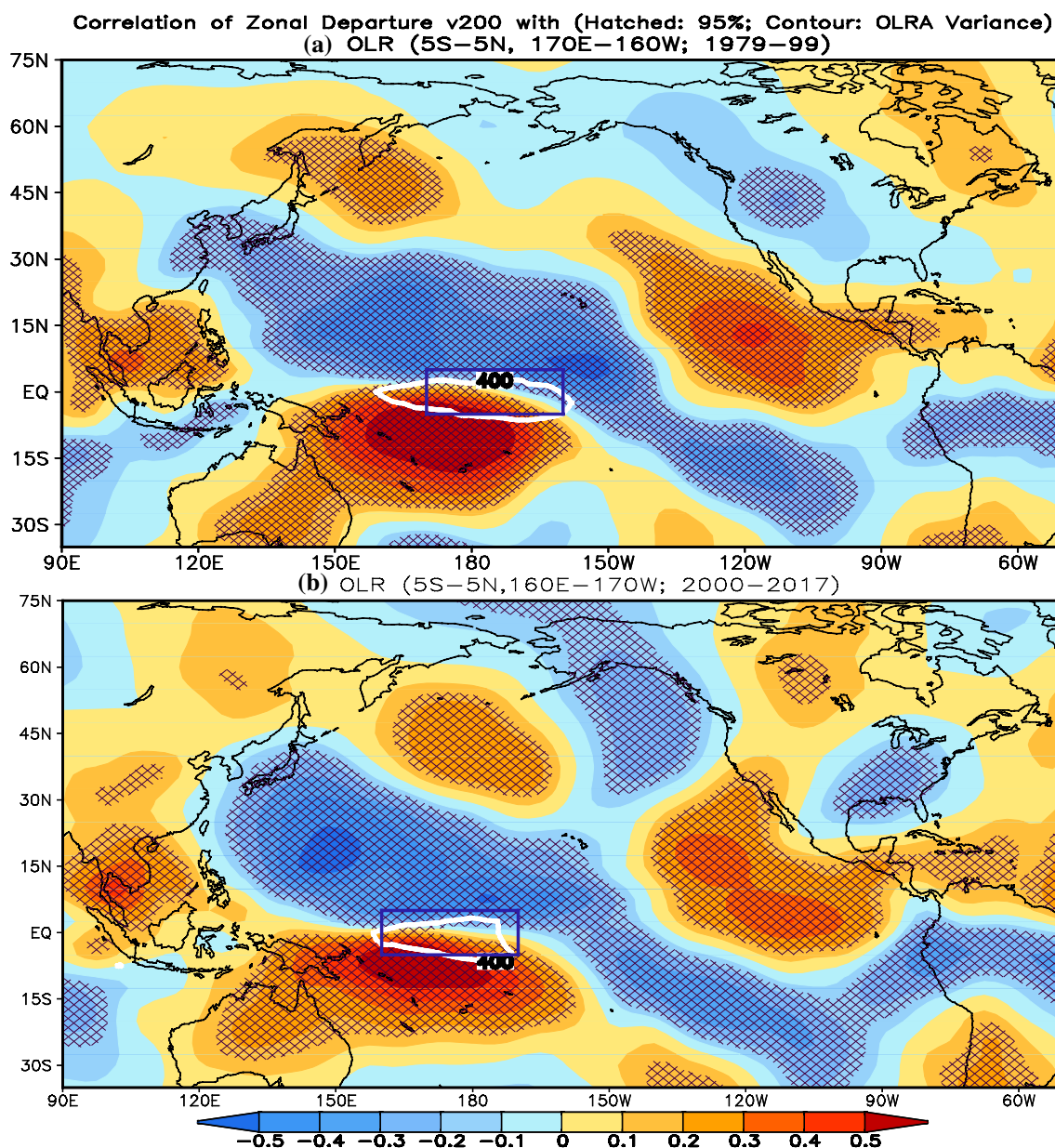


**Fig. 9** Correlations of zonal departure of meridional component of wind anomaly at 200 hPa ( $v_{200}$ ) with OLR anomaly averaged in **a** ( $5^{\circ}\text{S}$ – $5^{\circ}\text{N}$ ,  $170^{\circ}\text{E}$ – $160^{\circ}\text{W}$ ; see the rectangle) in January 1979–December 1999, and **b** ( $5^{\circ}\text{S}$ – $5^{\circ}\text{N}$ ,  $160^{\circ}\text{E}$ – $170^{\circ}\text{W}$ ; see the rectangle)

in January 2000–December 2017. The hatched regions represent significant at the 99% significance level, using a  $T$ -test. The contour of 400 is the variance of OLR anomalies in unit of  $(\text{W}/\text{m}^2)^2$ , which represents the most active convection regions

modifying the characteristics of ENSO, such as its spatial pattern, frequency, and intensity. However, the observed mean state changes from 1979 to 99 to 2000–2017 are not fully consistent with the consensus of model projections in the global warming scenario (Collins et al. 2010; Hu et al. 2016, 2017a). Thus, the observed mean state change from 1979–1999 to 2000–2017 may be also partially due to low-frequency variations of the atmosphere–ocean coupled system itself (Wittenberg 2009; Hu et al. 2012; Wang et al. 2016; Yu et al. 2015). Nevertheless, caution should be

exercised that the data period considered here may be rather short to deduce robust trends from observations (Harrison and Chiodi 2009, 2015; Ray and Giese 2012).

**Acknowledgements** The authors appreciate the constructive comments and insightful suggestions from reviewers. The procedure of the heat budget calculation used in this work was developed by Dr. Boyin Huang and is maintained by Dr. C. Wen. Prof. Li was supported by National Natural Science Foundation of China (41775040 and 41475039) and National Key Basic Research and Development Project of China (2015CB953601). The scientific results and conclusions, as

well as any view or opinions expressed herein, are those of the authors and do not necessarily reflect the views of NWS, NOAA, or the Department of Commerce.

## References

- An S-I, Wang B (2000) Interdecadal change of the structure of the ENSO mode and its impact on the ENSO frequency. *J Clim* 13:2044–2055
- Barnston AG, Tippett MK, L'Heureux ML, Li S, DeWitt DG (2012) Skill of real-time seasonal ENSO model predictions during 2002–2011—is our capability increasing? *Bull Am Meteorol Soc* 93(5):631–651
- Behringer DW (2007) The Global Ocean Data Assimilation System (GODAS) at NCEP. In: Preprints, 11th symposium on integrated observing and assimilation systems for atmosphere, oceans, and land surface, San Antonio, TX, Am Meteorol Soc, 3.3. [http://ams.confex.com/ams/87ANNUAL/techprogram/paper\\_119541.htm](http://ams.confex.com/ams/87ANNUAL/techprogram/paper_119541.htm). Accessed 16 Jan 2007
- Bellenger H, Guilyardi E, Leloup J, Lengaigne M, Vialard J (2014) ENSO representation in climate models: From CMIP3 to CMIP5. *Clim Dyn* 42(7–8):1999–2018. <https://doi.org/10.1007/s00382-013-1783-z>
- Bunge L, Clarke AJ (2014) On the warm water volume and its changing relationship with ENSO. *J Phys Oceanogr* 44:1372–1385
- Capotondi A, Wittenberg AT, Newman M, Di Lorenzo E, Yu J, Braconnot P, Cole J, Dewitte B, Giese B, Guilyardi E, Jin F, Karnauskas K, Kirtman B, Lee T, Schneider N, Xue Y, Yeh S (2015) Understanding ENSO Diversity. *Bull Am Meteorol Soc* 96:921–938. <https://doi.org/10.1175/BAMS-D-13-00117.1>
- Chen D, Lian T, Fu C, Cane MA, Tang Y, Murtugudde R, Wu Q, Zhou L (2015) A new perspective on ENSO classification and genesis. *Nat Geosci* 8:339–345. <https://doi.org/10.1038/ngeo2399>
- Chiang JCH, Vimont DJ (2004) Analogous Pacific and Atlantic meridional modes of tropical atmosphere-ocean variability. *J Clim* 17:4143–4158. <https://doi.org/10.1175/JCLI4953.1>
- Chiodi AM, Harrison DE (2015) Global seasonal precipitation anomalies robustly associated with El Niño and La Niña events—an OLR perspective. *J Clim* 28:6133–6159. <https://doi.org/10.1175/JCLI-D-14-00387.1>
- Collins M, An S-I, Cai W, Ganachaud A, Guilyardi E, Jin F-F, Jochum M, Lengaigne M, Power S, Timmermann A, Vecchi G, Wittenberg A (2010) The impact of global warming on the tropical Pacific Ocean and El Niño. *Nat Geosci* 3:391–397. <https://doi.org/10.1038/ngeo868>
- Garfinkel CI, Hurwitz MM, Waugh DW, Butler AH (2013) Are the teleconnections of Central Pacific and Eastern Pacific El Niño distinct in boreal wintertime? *Clim Dyn* 41:1835–1852
- Guan C, McPhaden MJ (2016) Ocean processes affecting the twenty-first-century shift in ENSO SST variability. *J Clim* 29:6861–6879. <https://doi.org/10.1175/JCLI-D-15-0870.1>
- Harrison DE, Chiodi AM (2009) Pre- and post-1997/98 westerly wind events and equatorial Pacific cold tongue warming. *J Clim* 22:568–581. <https://doi.org/10.1175/2008JCLI2270.1>
- Harrison DE, Chiodi AM (2015) Multi-decadal variability and trends in the El Niño–Southern Oscillation and tropical Pacific fisheries implications. *Deep-Sea Res II* 113:9–21. <https://doi.org/10.1016/j.dsr2.2013.12.020>
- Horii T, Ueki I, Hanawa K (2012) Breakdown of ENSO predictors in the 2000s: decadal changes of recharge/discharge—SST phase relation and atmospheric intraseasonal forcing. *Geophys Res Lett* 39:L10707. <https://doi.org/10.1029/2012GL051740>
- Hu S, Fedorov AV (2016) Exceptional strong easterly wind burst stalling El Niño of 2014. *Proc Natl Acad Sci USA* 113(8):2005–2010. <https://doi.org/10.1073/pnas.1514182113>
- Hu S, Fedorov AV (2018) Cross-equatorial winds control El Niño diversity and change. *Nat Clim Change* 8:798–802. <https://doi.org/10.1038/s41558-018-0248-0>
- Hu Z-Z, Kumar A, Jha B, Wang W, Huang B, Huang B (2012) An analysis of warm pool and cold tongue El Niños: air–sea coupling processes, global influences, and recent trends. *Clim Dyn* 38(9–10):2017–2035. <https://doi.org/10.1007/s00382-011-1224-9>
- Hu Z-Z, Kumar A, Ren H-L, Wang H, L'Heureux M, Jin F-F (2013) Weakened interannual variability in the tropical Pacific Ocean since 2000. *J Clim* 26(8):2601–2613. <https://doi.org/10.1175/JCLI-D-12-00265.1>
- Hu Z-Z, Kumar A, Huang B (2016) Spatial distribution and the interdecadal change of leading modes of heat budget of the mixed-layer in the tropical Pacific and the association with ENSO. *Clim Dyn* 46(5–6):1753–1768. <https://doi.org/10.1007/s00382-015-2672-4>
- Hu Z-Z, Kumar A, Huang B, Zhu J, Ren H-L (2017a) Interdecadal variations of ENSO around 1999/2000. *J Meteorol Res* 31(1), 73–81. <https://doi.org/10.1007/s13351-017-6074-x>
- Hu Z-Z, Kumar A, Zhu J, Huang B, Tseng Y, Wang X (2017b) On the shortening of the lead time of ocean warm water volume to ENSO SST since 2000. *Sci Rep* 7:4294. <https://doi.org/10.1038/s41598-017-04566-z>
- Hu Z-Z, Huang B, Zhu J, Kumar A, McPhaden MJ (2019) On the variety of coastal El Niño events. *Clim Dyn*. <https://doi.org/10.1007/s00382-018-4290-4> (published online)
- Huang B, Y. Xue, D. Zhang, A. Kumar, and M. J. McPhaden, 2010: The NCEP GODAS ocean analysis of the tropical Pacific mixed layer heat budget on seasonal to interannual time scales. *J Clim* 23(18):4901–4925.
- Huang B, Thorne PW, Banzon VF, Boyer T, Chepurin G, Lawrimore JH, Menne MJ, Smith TM, Vose RS, Zhang H-M (2017) Extended Reconstructed Sea Surface Temperature version 5 (ERSSTv5), Upgrades, validations, and intercomparisons. *J Clim* 30(20):8179–8205. <https://doi.org/10.1175/JCLI-D-16-0836.1>
- Jin F-F, Hoskins BJ (1995) The direct response to tropical heating in a baroclinic atmosphere. *J Atmos Sci* 52:307–319
- Kanamitsu M, Ebisuzaki W, Woollen J, Yang S-K, Hnilo JJ, Fiorino M, Potter GL (2002) NCEP–DOEAIIP—II reanalysis (R–2). *Bull Am Meteorol* 83:1631–1643
- Kessler WS, McPhaden MJ, Weickmann KM (1995) Forcing of intraseasonal Kelvin waves in the equatorial Pacific. *J Geophys Res* 100(C6):10613
- Kumar A, Hu Z-Z (2014) Interannual and interdecadal variability of ocean temperature along the equatorial Pacific in conjunction with ENSO. *Clim Dyn* 42(5–6):1243–1258. <https://doi.org/10.1007/s00382-013-1721-0>
- L'Heureux M, Collins D, Hu Z-Z (2013) Linear trends in sea surface temperature of the tropical Pacific Ocean and implications for the El Niño–Southern Oscillation. *Clim Dyn* 40(5–6):1223–1236. <https://doi.org/10.1007/s00382-012-1331-2>
- Li X, Hu Z-Z, Huang B (2019) Contributions of atmosphere-ocean interaction and low-frequency variation to intensity of strong El Niño events since 1979. *J Clim*. <https://doi.org/10.1175/JCLI-D-18-0209.1> (published online)
- Liebmann B, Smith CA (1996) Description of a complete (interpolated) outgoing long wave radiation dataset. *Bull Am Meteorol Soc* 77:1275–1277
- Lloyd J, Guilyardi E, Weller H, Slingo J (2009) The role of atmosphere feedbacks during ENSO in the CMIP3 models. *Atmos Sci Lett* 10:170–176

- Lübbecke JF, McPhaden MJ (2014) Assessing the 21st century shift in ENSO variability in terms of the Bjerknes stability index. *J Clim* 27:2577–2587
- McPhaden MJ (2012) A 21st century shift in the relationship between ENSO SST and warm water volume anomalies. *Geophys Res Lett* 39:L09706. <https://doi.org/10.1029/2012GL051826>
- National Research Council (2010) Assessment of intraseasonal to interannual climate prediction and predictability. The National Academies Press, Washington, DC, p 192
- Peng P, Kumar A, Hu Z-Z (2018) What drove Pacific and North America climate anomalies in winter 2014/15? *Clim Dyn* 51(7–8):2667–2679. <https://doi.org/10.1007/s00382-017-4035-9>
- Ray S, Giese BS (2012) Historical changes in El Niño and La Niña characteristics in an ocean reanalysis. *J Geophys Res* 117:C11007. <https://doi.org/10.1029/2012JC008031>
- Ren H-L, Jin F-F (2011) Niño indices for two types of ENSO. *Geophys Res Lett* 38:L04704. <https://doi.org/10.1029/2010GL046031>
- Seo K-H, Xue Y (2005) MJO-related oceanic Kelvin waves and the ENSO cycle: a study with the NCEP global ocean data assimilation system. *Geophys Res Lett* 32:L07712. <https://doi.org/10.1029/2005GL022511>
- Ting, M. and P.D. Sardeshmukh, 1993: Factors determining the extratropical response to equatorial diabatic heating anomalies. *J Atmos Sci* 50, 907–918. [https://doi.org/10.1175/1520-0469\(1993\)050<0907:FDERT>2.0.CO;2](https://doi.org/10.1175/1520-0469(1993)050<0907:FDERT>2.0.CO;2)
- Wang W, Chen M, Kumar A (2010) An assessment of the CFS real-time seasonal forecasts. *Wea Forecast* 25:950–969
- Wang C, Deser C, Yu J-Y, DiNezio P, Clement A (2016) El Niño–Southern Oscillation (ENSO): a review. In: Glynn P, Manzello D, Enochs I, (eds) *Coral reefs of the Eastern Pacific*. Springer Science Publisher, New York, pp 85–106
- Wen C, Kumar A, Xue Y, McPhaden MJ (2014) Changes in tropical Pacific thermocline depth and their relationship to ENSO after 1999. *J Clim* 27:7230–7249. <https://doi.org/10.1175/JCLI-D-13-00518.1>
- Wittenberg AT (2009) Are historical records sufficient to constrain ENSO simulations? *Geophys Res Lett* 36:L12702. <https://doi.org/10.1029/2009GL038710>
- Xiang B, Wang B, Li T (2013) A new paradigm for the predominance of standing Central Pacific warming after the late 1990s. *Clim Dyn* 41(2):327–340. <https://doi.org/10.1007/s00382-012-1427-8>
- Xie S-P, Philander SGH (1994) A coupled ocean–atmosphere model of relevance to the ITCZ in the eastern Pacific. *Tellus* 46A:340–350. <https://doi.org/10.1034/j.1600-0870.1994.t01-1-00001.x>
- Yang J, Peltier WR, Hu Y (2016) Monotonic decrease of the zonal SST gradient of the equatorial Pacific as a function of CO<sub>2</sub> concentration in CCSM3 and CCSM4. *J Geophys Res-Atmos* 121:637–610,653. <https://doi.org/10.1002/2016JD025231>
- Yeh S, Kug J, Dewitte B, Kwon M, Kirtman BP, Jin F-F (2009) El Niño in a changing climate. *Nature* 461(7263):511–514. <https://doi.org/10.1038/nature08316>
- Yu J-Y, Kao H-Y, Lee T, Kim ST (2011) Subsurface ocean temperature indices for central-Pacific and eastern-Pacific types of El Niño and La Niña events. *Theor Appl Clim* 103(3–4):337–344. <https://doi.org/10.1007/s00704-010-0307-6>
- Yu J-Y, Kao PK, Paek H, Hsu HH, Hung CW, Lu MM, An S-I (2015) Linking emergence of the central Pacific El Niño to the Atlantic multidecadal oscillation. *J Clim* 28(2):651–662

**Publisher's Note** Springer Nature remains neutral with regard to jurisdictional claims in published maps and institutional affiliations.